Climate Dynamics (1993) 8:277–285

Climate Dynamics

The effect of a regional increase in ocean surface roughness on the tropospheric circulation: a GCM experiment

Uwe Ulbrich[1], Gerd Bürger[2], Dierk Schriever[2], Hans von Storch[2], Susanne L Weber[3], Gerhard Schmitz[4]

[1] Institut für Geophysik und Meteorologie, Köln, Germany
[2] Max Planck Institut für Meteorologie, D-20146 Hamburg, Germany
[3] Koninklijk Nederlands Meteorologisch Instituut, De Bilt, The Netherlands
[4] Institut für Atmosphärenphysik, Kühlungsborn, Germany

Received: 6 September 1991 / Accepted: 13 January 1992

Abstract. The sensitivity of the atmospheric circulation to an increase in ocean surface roughness in the Southern Hemisphere storm track is investigated in a paired general circulation model experiment. Such a change in sea roughness could be induced by ocean waves generated by storms. Two extended permanent-July runs are made. One with standard sea surface roughness, the other with ten times as a large surface roughness over open sea poleward of 40° S. The regional increase in ocean surface roughness significantly modifies the tropospheric circulation in the Southern Hemisphere. The strongest effect is the reduction of tropospheric winds (by 2 m/s or 10%) above the area with increased roughness. The poleward eddy momentum flux is reduced in the upper troposphere and the meridional eddy sensible heat flux is reduced in the lower troposphere. Zonal mean and eddy kinetic energy are consistently reduced.

1 Introduction

Surface fluxes of momentum and heat are important processes in the parameterization package of a general circulation model (GCM). A characteristic parameter in the parameterization of these fluxes is the surface roughness length or, equivalently, the neutral drag coefficient. It is not clear whether the model circulation is sensitive to variations of these parameters. A global doubling of the roughness length has little impact on the atmospheric circulation (Miller et al. 1989).

A regional, instead of a global, modification of the surface roughness may have a significant impact on the atmospheric circulation. Kitoh and Yamazaki (1991) and Sud and Smith (1985) indeed found a stronger atmospheric circulation in the tropics, related to enhanced latent heat fluxes, as a response to increased roughness in the tropics.

In primitive equation models the atmospheric circulation is sensitive to changes in the surface fluxes. James and Gray (1986) find that increasing the drag coefficient by a factor of ten and more induces lower zonal and higher eddy energies. On the other hand, Branscome et al. (1989) found a reduction of all energy reservoirs as a response to the inclusion of surface fluxes in their model.

In the present study, we investigate an increase of ocean surface roughness in the Southern Hemisphere storm track. Our motivation was related to the interaction between the atmospheric boundary layer and gravity waves generated on the ocean surface. Field data show that the surface momentum flux is enhanced directly after a sudden change in the surface winds, because new waves are generated (Donelan 1982; Maat et al. 1991). In the very initial stage of wave growth the roughness length can be enhanced by as much as a factor of ten (Janssen 1989). The effect of wave growth is expected to be most pronounced in the storm tracks, where the surface winds are strongest and have maximum variability. In an idealized sensitivity experiment we investigate whether the atmospheric circulation is modified by such an increase in the sea roughness. We enhanced the surface roughness uniformly, southward of 40° S, by a constant factor of ten. In the present study, we compare the circulation in this idealized sensitivity experiment with the circulation obtained in a control experiment. In the discussion we come back to the question of whether our experimental set-up is adequate to describe the effect of ocean wave generation.

The design of the GCM experiment and the statistical techniques employed are described in Section 2. In Section 3 the results of the experiment are presented: first the statistical stability of the signal is investigated; then the effect of the regionally enhanced surface roughness on the time-mean fields, on the eddy fields and on the atmospheric energy cycle is studied. In Section 4 the paper is concluded with a discussion of the dynamic processes involved and of the significance of our experiment for the parameterization of the momentum flux from the atmospheric flow to the ocean wave field.

Correspondence to: H von Storch

2 Technical preliminaries

The GCM runs

We use a low resolution GCM, called ECHAM1, which is a modified version of the ECMWF operational numerical weather prediction model adapted for climate simulation purposes (Roeckner et al. 1989). The horizontal grid, on which surface processes are calculated, is a 64 longitude × 32 Gaussian latitude grid. The vertical discretization consists of 19 unevenly distributed hybrid levels.

The roughness length z_0 of the ocean surface is given in the GCM by the Charnock (1957) formula, modified by a minimum condition:

$$z_0 = \max\left[\alpha \frac{\tau}{g\rho};\ 0.15\ \text{mm}\right]$$

where τ is the magnitude of the turbulent surface stress, g is the gravitational constant, ρ is the density of air and α is a tunable proportionality constant. The minimum roughness represents the limit of viscous flow. For a neutral stratification the roughness length is related to the drag coefficient c_D at height z by:

$$c_D(z) = (0.4/\ln(z/z_0))^2$$

In the case of a nonneutral atmosphere this coefficient is modified using a factor which depends on the Richardson number.

Two experiments were performed: one with the standard $\alpha = 0.018$ everywhere, and the other with the same $\alpha = 0.018$ north of 40° S and the tenfold $\alpha = 0.18$ over the open ocean south of 40° S. Both runs were made under "permanent-July" conditions. Such a model run without an annual cycle yields a comparatively large number of samples. The Southern Hemisphere winter month is chosen because maximum surface wind variability is observed over the Southern Ocean at that time (Trenberth and Olson 1988). Both runs were integrated over 24 months. The first 4 months of the control run and of the experimental run are not used in the analysis in order to exclude possible effects of initial values.

The time-mean difference of the roughness in the experiment and the roughness in the control run is shown in Fig. 1. In the area where α was not changed, z_0 is almost unchanged. In the 40°–60° S belt z_0 is enhanced by 2–3 mm. Maximum increases of 5 mm are in the Indian Ocean.

Statistics

The prerequisite for any *physical* discussion is the existence of a statistically significant signal in the simulated data, i.e., the certainty that the differences between the two runs are due to the experimental change and that they do not reflect random fluctuations.

Hasselmann (1979) proposed a general procedure to identify a statistically significant signal in a noisy, high-dimensional environment. The procedure was shown to be useful by, among others, Hannoschöck and Frankignoul (1985), von Storch (1987) and Hense et al. (1990). Its general idea is to project the raw data onto a low-dimensional space which we hope contains the signal. The selection of this low-dimensional space may be done in a hierarchical manner such that the significance and the statistical stability of the signal are optimized. In the second step of the procedure, a multivariate statistical test is applied to the reduced data. The fact that this is done in a low-dimensional space increases the power of the test and facilitates the detection of the signal when the signal-to-noise ratio is small. After having ascertained the reality of the signal, a further analysis of the statistical stability of the regional details of the (high-dimensional) signal is often useful.

In the following, we outline some aspects of the signal-detection strategy that we have used in our study in more detail. In this analysis we consider $\mathbf{x}$ and $\mathbf{y}$, which denote the two d dimensional vectors representing the control run and the experimental run. In the present study they are the latitude-height distribution of the zonally averaged time-mean zonal wind. There are n realizations $\mathbf{x}(i)$ of $\mathbf{x}$ and m realizations $\mathbf{y}(i)$ of $\mathbf{y}$. The mean over the $n(m)$ realizations of $\mathbf{x}(\mathbf{y})$ is $\bar{\mathbf{x}}(\bar{\mathbf{y}})$.

Guess patterns. In our example d is of the order 100 or more and n and m are of the order 10. We can reduce the number of degrees of freedom using *guess patterns* with dimension k, where $k \ll d$ (Hasselmann 1979). The a priori chosen patterns are expected to describe the signal as well as possible. The data are projected onto this k dimensional *guess space*, where the multivariate statistical tests are performed. If there is a statistically significant signal in the low dimensional guess space, the multivariate signal itself is restored by expansion in the guess patterns. The resulting signal S_k in the full space is called the *filtered signal.* A measure of the power of the filtered signal is the *explained variance* of the full signal, i.e., the percentage of the variance of the full signal that is explained by the filtered signal.

The tests need not be done in only one k dimensional guess space. In the *hierarchical* mode (Barnett et al. 1981) a maximum number K of guess patterns is selected, and the test is done in the series of guess spaces spanned by the first k guess-patterns, $k = 1, \ldots, K$, consecutively.

There are several strategies to obtain guess-patterns (von Storch 1987; Hense et al. 1990). In the present study we use empirical orthogonal functions (EOFs) and we order them according to descending eigenvalue.

Multivariate Hotelling test. The Hotelling test or multivariate t-test (e.g., Morrison 1976) evaluates the null-hypothesis $\mu_x = \mu_y$, with μ_x and μ_y denoting the expectations of $\mathbf{x}$ and $\mathbf{y}$. One assumes that $\mathbf{x}$ and $\mathbf{y}$ are normally distributed with equal variances. Given the distribution of $\mathbf{x}$ the Hotelling test evaluates the probability to draw m samples $\mathbf{z}(i)$ from $\mathbf{x}$, with a mean $\bar{\mathbf{z}}$, such that $|\bar{\mathbf{z}} - \bar{\mathbf{x}}|^2$ is larger than or equal to $|\bar{\mathbf{y}} - \bar{\mathbf{x}}|^2$. If this probability is below the a priori specified risk the null-hypothesis is rejected. The Hotelling test statistic is defined as:

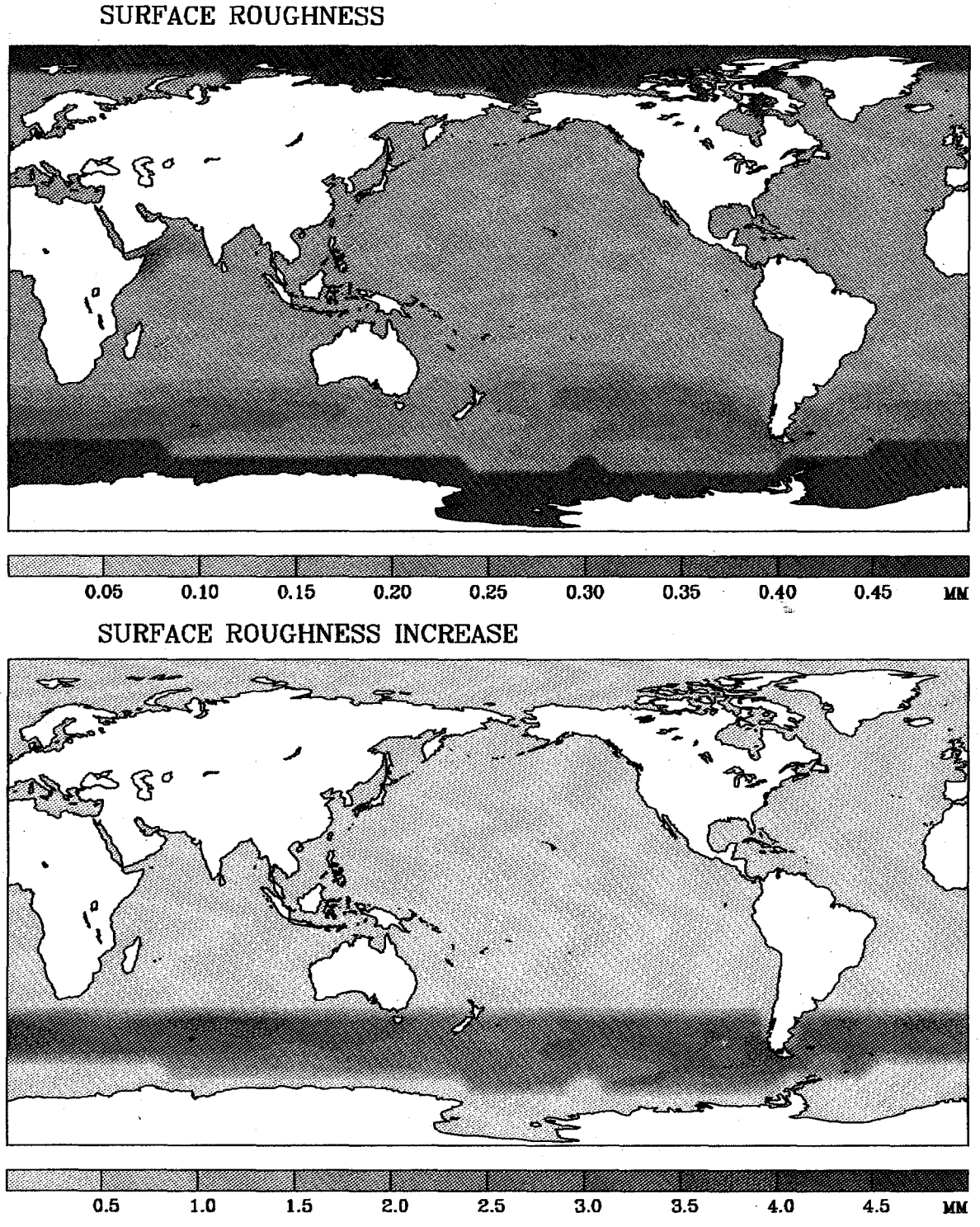

Fig. 1. The global distribution of ocean surface roughness (in mm) in the ECHAM atmospheric GCM: *Top:* the time-mean field in the control run; *Bottom:* the difference experiment minus control

$$T^2 = \frac{n \cdot m}{n+m} \cdot (\bar{\mathbf{x}} - \bar{\mathbf{y}})^t \cdot \Gamma^{-1} \cdot (\bar{\mathbf{x}} - \bar{\mathbf{y}})$$

Here ^{t} denotes the transpose and Γ is the estimated pooled covariance matrix of the ensembles:

$$\Gamma = \frac{1}{n+m-2} \cdot \left(\sum_{i=1}^{n} (\mathbf{x}(i) - \bar{\mathbf{x}}) \cdot (\mathbf{x}(i) - \bar{\mathbf{x}})^t + \sum_{i=1}^{m} (\mathbf{y}(i) - \bar{\mathbf{y}}) \cdot (\mathbf{y}(i) - \bar{\mathbf{y}})^t \right)$$

Note that the matrix Γ is regular if $d > n+m-2$. Up to some scaling factor, T^2 is Fisher-F distributed if the null-hypothesis holds. Thus, we reject the null-hypothesis $\mu_x = \mu_y$ at the α-th level, or, with a *risk* of $(1-\alpha)$ if:

$$T^2 > \frac{(n+m-2) \cdot d}{n+m-d-1} \cdot F_{\alpha;\, d,\, n+m-d-1}$$

where $F_{\alpha;\,d,n+m-d-1}$ denotes the α-quantile of the Fisher distribution with d and $n+m-d-1$ degrees of freedom.

If the null-hypothesis $\mu_x=\mu_y$ has been rejected, the difference $\bar{\mathbf{y}}-\bar{\mathbf{x}}$ is called the *significant signal.*

Multivariate recurrence analysis. A small risk of erroneously rejecting the null-hypothesis does not imply that the samples are well separated and that the signal is strong. If very many samples are available the power of a test to detect even small differences becomes large. The parameter *level of recurrence* (Zwiers and von Storch 1989) measures the discrimination between the control sample and the experimental sample. To obtain this parameter the space is split up into two disjoint sets Ω_x and Ω_y, so that the probability for any realization $\mathbf{x}$ to be in Ω_x and for any realization $\mathbf{y}$ to be in Ω_y is maximum:

$$\text{Prob}(\mathbf{x}\in\Omega_x)=\text{Prob}(\mathbf{y}\in\Omega_y)=p$$

Since Ω_x and Ω_y are disjoint the probability for any $\mathbf{x}$ to hit Ω_y or for any $\mathbf{y}$ to hit Ω_x is minimum:

$$\text{Prob}(\mathbf{y}\in\Omega_x)=\text{Prob}(\mathbf{x}\in\Omega_y)=1-p$$

The larger the *level of recurrence* p is, the smaller is the overlap between the two distributions over the control sample and the experimental sample. An alterative interpretation is: if the level of recurrence is p and if $\mathbf{z}$ is drawn randomly either from $\mathbf{x}$ or from $\mathbf{y}$, then the chance to guess the origin of $\mathbf{z}$ correctly is p.

Test hierarchies. For each of the guess spaces, spanned by the first k guess patterns, the risk $(1-\alpha_k)$ of rejecting the null-hypothesis and the level of recurrence p_k are derived. If it is possible to find a $k<n+m-2$ such that $\alpha_k\geqslant 99\%$, we choose the filtered signal S_k which has maximum recurrence p_k as the *significant* filtered signal. Hence, S_k will be optimal with respect to significance and recurrence.

Serial correlation. Stastistical tests, as the Hotelling test, operate on sets of *independent and identically distributed* samples. In our experiments the GCM is integrated in the permanent-July mode. Removing any trend and forming T-day means (i.e., means taken over T consecutive days) gives identically distributed samples. However, due to serial correlation these samples are, in general, *not* independent.

There are two ways of dealing with this serial correlation. One approach is to form T-day means not from adjacent T-day intervals, but to use instead intervals of length $T+\delta$. Then the mean of the first T days of each interval of length $T+\delta$ is calculated. Here δ is the time after which the atmospheric fields lose their memory, i.e., the time after which the auto-correlation has decreased to zero. After Gutzler and Mo (1983) and Trenberth (1985) $\delta=10$ days is an adequate choice. The other approach is to perform the statistical test as usual, but to use a corrected value for the number of test samples (realizations). If N is the total length of a time series, then $n=N/T$ samples are available. The number of *independent* samples, which are contained in the total of all samples, is $n^*=n\cdot T/(T+\delta)=N/(T+\delta)$. Therefore, with $N=600$ and $\delta=10$, we find with both approaches that the number of independent samples is 15 for $T=30$ days, whereas it is 30 for $T=10$ days.

Local analyses. After having identified a significant filtered signal S_k by means of the multivariate Hotelling test and the multivariate recurrence analysis in one physical quantity, we proceed with local analyses at each grid point. The statistical stability of the signal in other quantities is examined locally by the t-test, using adjacent 30-day intervals and an adjusted number of test samples $n^*=m^*=15$.

3 Results

We applied the statistical analysis outlined in the previous section to our GCM experiments in order to determine if the model climate has significantly changed as a result of the enhanced ocean surface roughness in the Southern Hemisphere storm track.

A zonally averaged quantity is denoted by []-brackets, whereas the deviation from the zonal mean is denoted by a prime. A "mean" refers to a time-mean and is denoted by an overbar.

Identification of a statistically significant signal

We consider the latitude-height distribution of the zonally averaged time-mean zonal wind, denoted by $[\bar{u}]$, taken at ten pressure levels between 1000 hPa and 20 hPa, and at seventeen Gaussian latitudes between 25° N and 65° S. We concentrate the analysis on the Southern Hemisphere because we anticipate the signal to be primarily in the Southern Hemisphere.

In a first attempt, we select the variables $\mathbf{x}$ and $\mathbf{y}$ to be *monthly* means, i.e., $T=30$ days. Then, $n=m=15$ independent samples are available. The risks $(1-\alpha_k)$ of erroneously rejecting the null-hypothesis of equal means, is larger than 20% for all $K=n+m-3=27$ elements in the hierarchy of guess spaces (not shown).

With $T=10$ days, $n=m=30$ independent samples are available, and the hierarchy length is $K=57$. This choice of T leads to a marked improvement of the power of the Hotelling-test (Fig. 2). S_{30} is chosen as the significant filtered signal, because $p_{30}=82\%$ is maximum and $\alpha_{30}>99\%$; S_{30} explains 97% of the variance of the full signal. The filtered signal (Fig. 3) represents a weakening of the zonal mean circulation. In the troposphere there is a easterly anomaly between 40° S and 70° S and a westerly anomaly between 30° S and 10° N. The pattern is reversed in the stratosphere.

Local analyses of the signal

Now that the existence of a significant signal has been established, we continue our analysis with local tests of monthly mean fields.

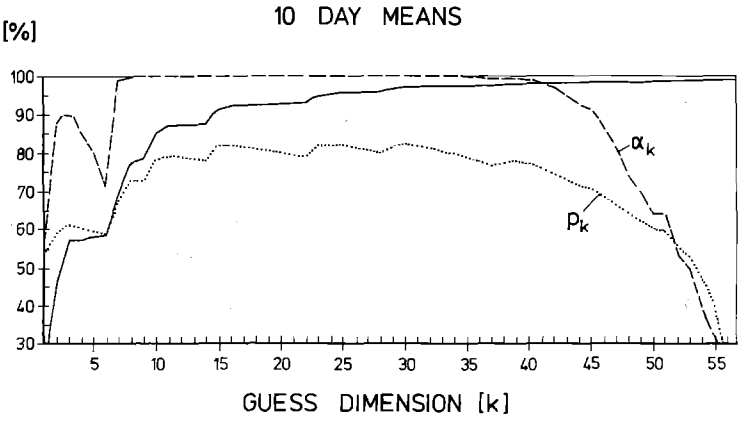

Fig. 2. Multivariate analysis of the signal (experiment minus control) in the zonally averaged 10-day mean zonal wind [ū] in the Southern Hemisphere: the signal is projected onto the guess-space spanned by the first k EOFs ($k=1....57$) and the significance levels α_k (*dashed*), levels of recurrence p_k (*dotted*) and explained variance (*solid*) are computed as functions of the hierarchy parameter k

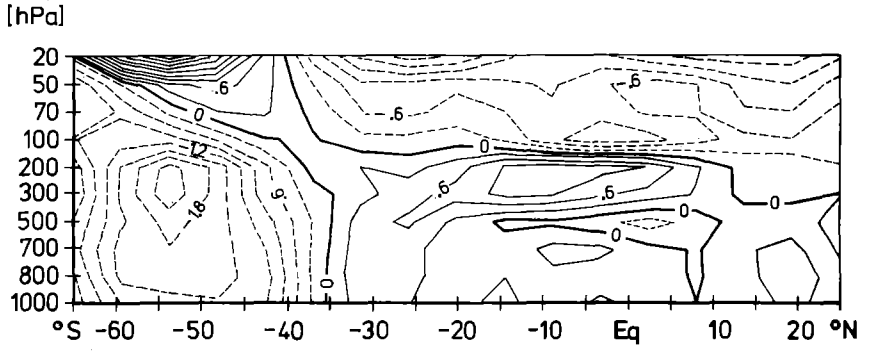

Fig. 3. The significant filtered response S_{30} (experiment minus control) of the zonally averaged 10-day mean zonal wind [ū] to the enhanced ocean surface roughness south of 40° S. The risk $(1-\alpha_{30})$ that S_{30} is merely reflecting random variations is less than 1%; S_{30} is associated with a recurrence-level p_{30} of 82%

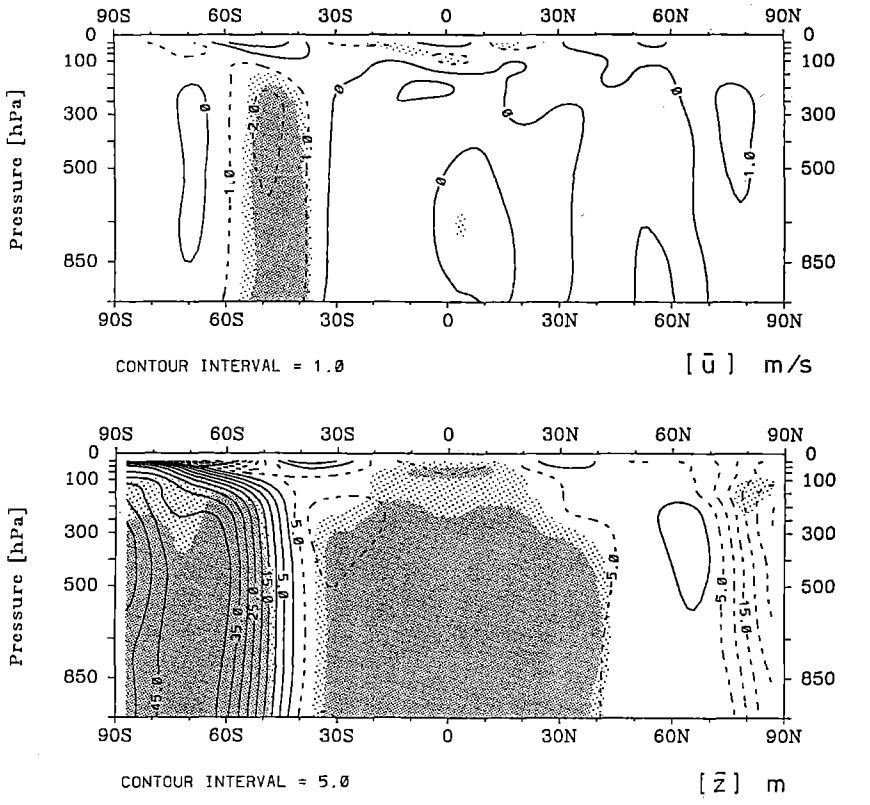

Fig. 4. The latitude-height distribution of the difference (experiment – control) in the zonally averaged time-mean field of the zonal-wind ([ū]; units: m/s; *top*), and of the geopotential height ([z̄]; units: gpm; *bottom*). Differences which are locally significant at the 5% (1%) level are indicated by *light* (*heavy*) shading

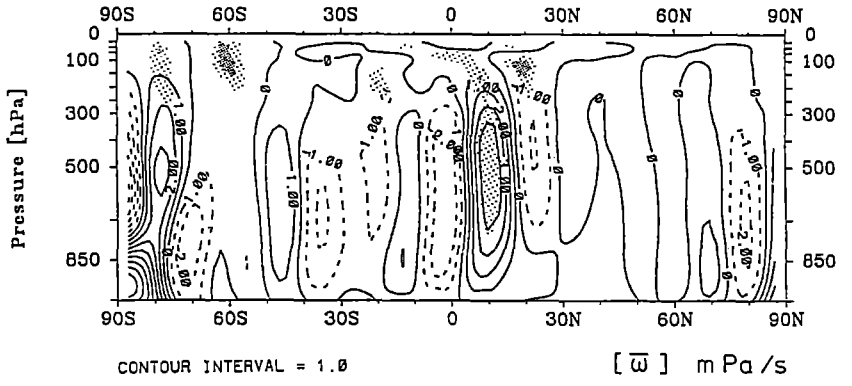

Fig. 5. The latitude-height distribution of the difference (experiment – control) in the zonally averaged time-mean vertical ω-wind ($[\bar{\omega}]$; units: 10^{-3} Pa/s). Differences which are locally significant at the 5% (1%) level are indicated by *light* (*heavy*) shading

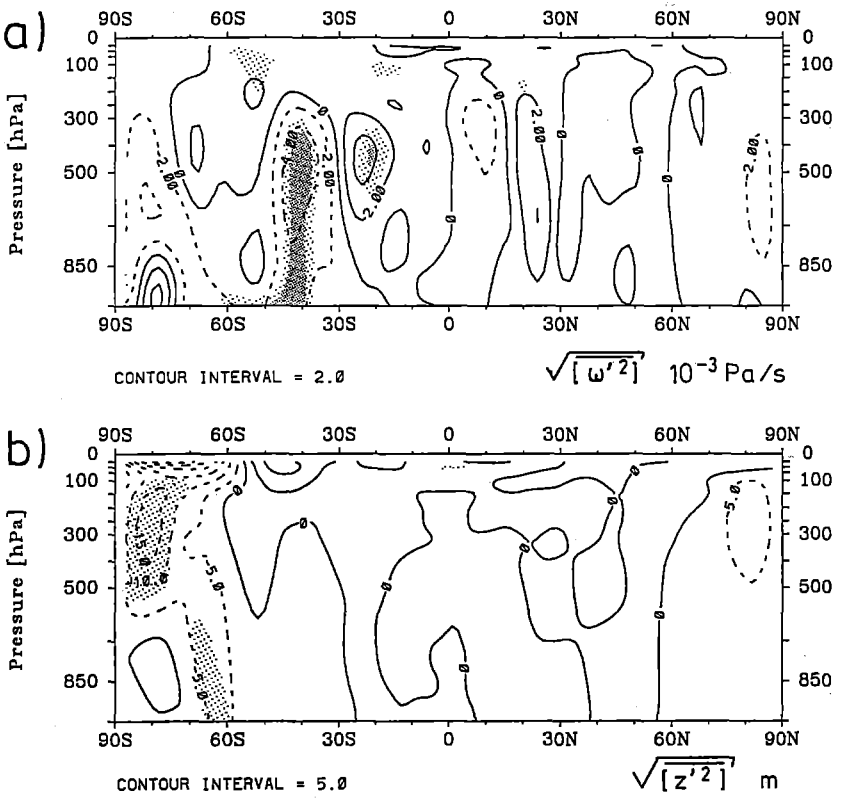

Fig. 6a, b. The latitude-height distribution of the difference (experiment – control) in the zonally averaged time-mean eddy fields of **a** the vertical ω-wind ($[\overline{\omega'^2}]^{1/2}$; units: 10^{-3} Pa/s), **b** the geopotential height ($[\overline{z'^2}]^{1/2}$; units: gpm). Differences which are locally significant at the 5% (1%) level are indicated by *light* (*heavy*) shading

Latitude-height distribution of zonally averaged time-mean fields. As expected, the full signal (experiment minus control) in the zonal wind [ū] (Fig. 4) is very similar to the filtered signal (Fig. 3). A maximum reduction in the zonal wind, by more than 2 m/s (or 10%), is found in the area above the increased surface roughness. The tropospheric pattern has only little vertical variations and is, according to the local *t*-test, statistically highly stable. The decrease of the zonal wind in the storm track is consistently reflected in the hemispheric mass distribution (Fig. 4). Being in geotrophic balance, geopotential heights have increased (decreased) at all latitudes poleward (equatorward) of 40° S.

Meridional temperature contrasts in the Southern Hemisphere are not altered (not shown). The temperature has increased (decreased) by about 0.5 K below (above) 500 hPa south of 30° N, which implies a reduction in the static stability. This signal is associated with slightly increased low level humidity (not shown). The vertical velocity [$\bar{\omega}$] (Fig. 5) and the meridional velocity [$\bar{v}$] (not shown) have slightly decreased above the regions with increased roughness. Apart from these local effects, the anomalies in [$\bar{v}$] and in [$\bar{\omega}$] indicate a 5%–10% weakening of the Hadley cell. This weakening is marginally stable.

Latitude-height distribution of zonally averaged eddy fields. Here we examine the eddy variance. In the Southern Hemisphere the transient eddies contribute most to the eddy variance.

The eddy signals in the horizontal and vertical wind components (Fig. 6a), in the geopotential height (Fig. 6b) and in the temperature are similar. The most prominent feature is the reduction of eddy intensity in the storm track (by about 5%), and at higher levels above the Antarctic. A signal in the vertical wind, which is not observed in the other quantities, is an increase close to 20° S. This indicates an equatorward shift of the area of

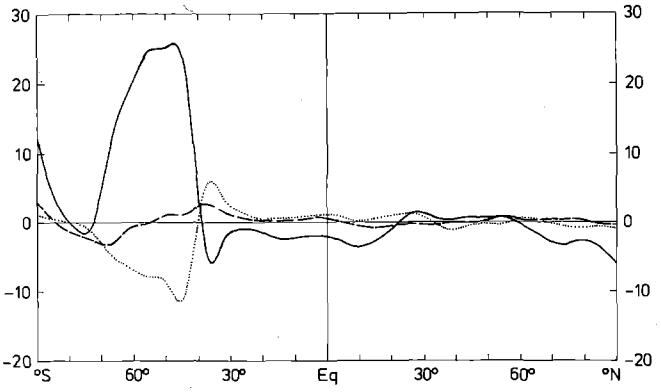

Fig. 7. The difference (experiment - control) in the zonally averaged time-mean surface fluxes of momentum (*solid*, in mPa), sensible heat (*dashed*, in Wm^{-2}) and latent heat (*dotted*, in Wm^{-2})

maximum variability in addition to the local weakening of the mean vertical wind (Fig. 5).

Consistent with these results, an analysis of the 2–15 day band-pass filtered variance of the 500 hPa geopotential shows reduced storminess over most of the Southern Hemisphere (not shown).

Zonally averaged surface fluxes. The surface momentum and latent heat flux have increased (by 5–10%) in the Southern Hemisphere storm track, whereas the surface sensible heat flux has hardly changed (Fig. 7). The relative changes are much smaller than what would result from a mere doubling of the exchange coefficients with the atmospheric circulation fixed.

The atmospheric energy cycle. We computed the energy reservoirs and conversions of the atmospheric energy cycle (Lorenz 1955; Saltzman 1957), using the formulation of Arpe et al. (1986). The globally averaged energy cycle describes the conversion from zonal mean available potential energy (*AZ*, determined by the zonally averaged meridional temperature contrasts) to eddy available potential energy (*AE*, determined by temperature contrasts along latitude circles) and further to eddy kinetic energy (*KE*) and to zonal mean kinetic energy (*KZ*). The two baroclinic conversions (from *AZ* to *AE*, and from *AE* to *KE*) are determined by the meridional and vertical eddy sensible heat flux, respectively. The barotropic conversion (from *KE* to *KZ*) is due to the meridional eddy momentum flux. Diabatic heating and frictional dissipation are not considered in this subsection, as they are not provided as model output.

The globally averaged terms of the atmospheric energy cycle are almost unaffected by the increase of the surface roughness. However, in the Southern Hemisphere there are locally significant changes in the energy reservoirs and the physical processes associated with the energy conversions. The baroclinic conversions from *AZ* to *AE* (not shown) and from *AE* to *KE* (Fig. 8a) as well as the reservoir *AE* (not shown) are reduced above the area with increased roughness and at the Antarctic coast. The barotropic conversion from *KE* to *KZ* has decreased in intensity (Fig. 8b). Consistent with the reduction in eddy and zonal mean wind speeds described earlier, the energy reservoirs *KZ* and *KE* are significantly reduced at all tropospheric levels between 30° S and 60° S (not shown).

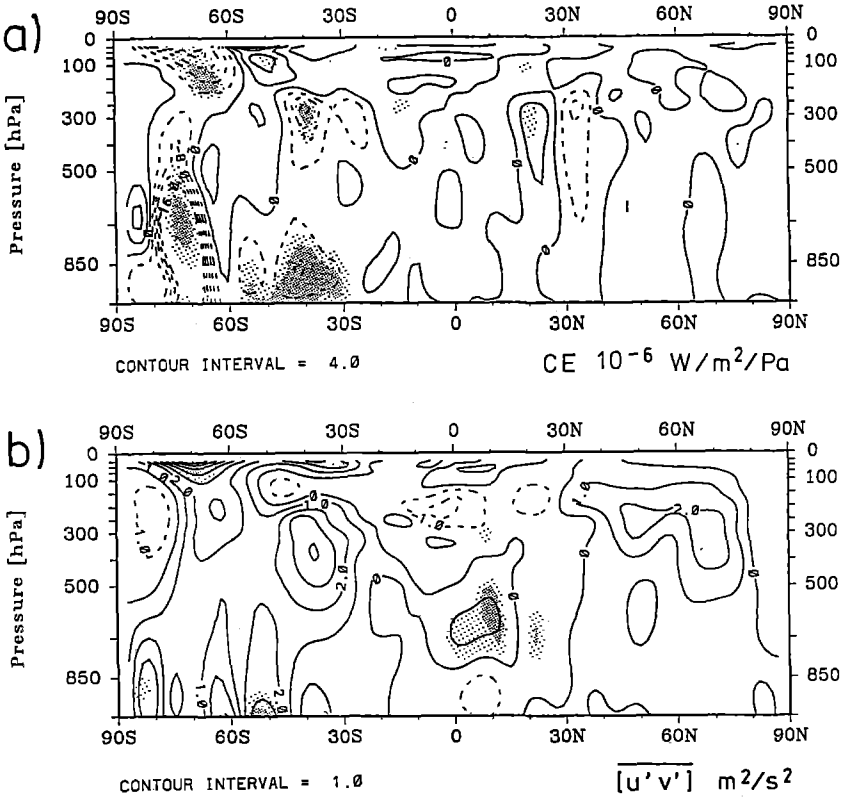

Fig. 8a, b. The latitude-height distribution of the difference (experiment - control) in the zonally averaged time-mean energy conversions: **a** the vertical eddy heat flux from the reservoir *AE* (eddy available potential energy) to the reservoir *KE* (eddy kinetic energy) $(-Rg^{-1}p^{-1}[\omega'T'];$ units: 10^{-6} $Wm^{-2}Pa^{-1})$, **b** the meridional eddy momentum flux from the reservoir *KE* (eddy kinetic energy) to the reservoir *KZ* (zonal mean kinetic energy) $(\overline{[u'v']};$ units: $m^2s^{-2})$. Differences which are locally significant at the 5% (1%) level are indicated by *light* (*heavy*) shading

4 Discussion and conclusions

The enhanced ocean surface roughness south of 40° S slows down the atmospheric circulation at all levels between 10° N and 70° S. This signal is globally significant. Local analyses show that a signal is visible in almost every atmospheric parameter. The largest impact is above the area of roughness enhancement, where both the zonal mean and the eddy activity is reduced.

In order to understand the dynamic response of the tropospheric circulation to the increased ocean surface roughness, we relate the enhancement of z_0 step by step to the reduction of the zonal mean wind. The direct effect of the enhanced roughness is to increase the surface latent heat flux, one of the sources for eddy available potential energy, and to increase the surface momentum flux, a sink for eddy and zonal mean kinetic energy. The direct effect of the enhanced surface friction, a decrease of the low level circulation, is observed. The indirect effects are less obvious: the increased roughness affects the development of baroclinic eddies, which interact with the mean circulation.

Branscome et al. (1989) examined the nonlinear development of baroclinic waves. They found that increased surface heat fluxes and increased friction causes a reduction of the meridional eddy sensible heat flux in the lower troposphere and of the meridional eddy momentum flux in the upper troposphere, as well as reduced eddy energies. The meridional and the vertical eddy sensible heat fluxes and the eddy available potential energy often show a similar response to changed boundary conditions (Ulbrich and Speth 1991).

Using a linear quasi-geostrophic model Dethloff and Schmitz (1982) related anomalous eddy momentum fluxes to anomalous zonal mean flow. They found that a weakened poleward eddy momentum flux at upper levels induces an easterly anomalous wind equatorward of the momentum-flux forcing and a westerly anomalous wind poleward of it. The anomalous patterns of the tropospheric wind (Fig. 4a) and of the eddy momentum flux (Fig. 8b) in our GCM experiment are qualitatively consistent with Dethloff and Schmitz's findings (see their Figs. 5 and 2). Also the magnitude of the anomalies (1–3 ms^{-1} in wind speed and 3–4 $m^2 s^{-2}$ in momentum flux) agree with Dethloff and Schmitz's results.

We propose that the tropospheric response in our experiment is controlled by two processes. One process is the direct impact of the enhanced roughness on the low-level zonal mean circulation. The other process consists of two steps. The increased roughness weakens the eddy fields and the meridional eddy momentum flux, which again weakens the mean zonal flow.

Our motivation for the present study was to examine the sensitivity of the atmospheric circulation to wave growth. Since wind waves are generated by storms we enhanced the ocean surface roughness uniformly in the Southern Hemisphere storm track. Parallel to the present study Weber et al. (1993) coupled a full ocean wave model to the ECHAM atmospheric GCM. They found that on a day-to-day basis the roughness enhancement showed complicated spatial and temporal patterns, reflecting the individual storms instead of the storm track. However, in less than 5% of the time the roughness enhancement was somewhat more than a factor two. The time-mean ocean surface roughness was fairly uniformly enhanced in the Southern Hemisphere storm track, but the enhancement (about 20%) was much weaker than assumed here. Wave growth did not have a significant impact on the climatological mean circulation.

We conclude that the atmospheric circulation is indeed sensitive to an enhancement of the ocean surface roughness in the storm tracks. However, the enhancement factor which we used cannot be related to wave growth, as the coupled wave AGCM experiments show that, in realistic simulations, wave growth results in a sea roughness enhancement of a factor two at most. This is too small to cause the effects which we observe in the present experiments.

Acknowledgements. We thank the ECHAM group at the Meteorological Institute of the University of Hamburg for thoroughly preparing the GCM and offering it to the scientific community as a readily accessible community model. We are particularly grateful to Ulrich Schlese and Ulrich Cubasch who helped us to realize our experimental design. Peter Janssen gave advice; Andreas Hense supplied us with his statistical software package. The project was in part financed by the EC through project EPOC 0003-C and by the BMFT through projects 07 KFT 306 and 07 KFT 012.

References

Arpe K, Brancovic C, Oriol E, Speth P (1986) Variability in time and space of energetics from a long time series of atmospheric data produced by ECMWF. Beitr Phys Atmos 59:321–355

Barnett TP, Preisendorfer RW, Goldenberg LM, Hasselmann KH (1981) Significance tests for regression model hierarchies. J Phys Oceanogr 11:1150–1154

Branscome LE, Gutowski WJ, Stewart DA (1989) Effect of surface fluxes on the nonlinear development of baroclinic waves. J Atmos Sci 46:460

Charnock H (1955) Wind stress on a water surface. Quart J R Meteorol Soc 81:639

Dethloff K, Schmitz G (1982) On determining the tropo- and stratospheric zonal circulation on the basis of momentum and heat sources in a quasi-geostrophic model. Part I. Gerlands Beitr Geophys 91:25–34

Donelan M (1982) The dependence of the aerodynamic drag coefficient on wave parameters. Proc First Int Conf on Meteorology and air-sea interaction of the coastal zone. The Hague, Am Meteorol Soc, pp 381–387

Gutzler D, Mo K (1983) Autocorrelation of northern hemisphere geopotential heights. Mon Weather Rev 111:155–164

Hannoschöck G, Frankignoul C (1985) Multivariate statistical analysis of a sea surface temperature anomaly experiment with the GISS general circulation model. J Atmos Sci 42:1430–1450

Hasselmann K (1979) On the signal-to-noise problem in atmospheric response studies. Meteorology over the tropical oceans. R Soc London, pp 251–258

Hense A, Glowienka-Hense R, von Storch H, Stähler U (1990) Northern Hemisphere atmospheric response to changes of Atlantic Ocean SST on decadal time scales: A GCM experiment. Clim Dyn 4:157–174

James IN, Gray LJ (1986) Concerning the effect of surface drag on the circulation of a baroclinic planetary atmosphere. Quart J R Meteorol Soc 112:1231–1250

Janssen PAEM (1989) Wave-induced stress and the drag of air flow over sea waves. J Phys Oceanogr 19:745–754

Kitoh A, Yamazaki K (1991) Impact of surface drag of islands in the Maritime Continent on the atmospheric general circulation. J Meteorol Soc Japan 69:241–248

Lorenz NL (1955) Available potential energy and the maintenance of general circulation. Tellus 7:157–167

Maat N, Kraan C, Oost WA (1991) The roughness of wind waves. Boundary-Layer Meteorol 54:89–103

Miller MJ, Palmer TN, Swinbank R (1989) Parameterization and influence of subgridscale orography in general circulaltion and numerical weather prediction models. Meteorol Atmos Phys 40:84–109

Morrison DF (1976) Multivariate statistical methods. McGraw-Hill, Singapore, pp 1–415

Roeckner E, Dümenil L, Kirk E, Lunkeit F, Ponater M, Rockel B, Sausen R, Schlese U (1989) The Hamburg version of the ECMWF model (ECHAM). GARP Report 13, WMO Geneva, WMO/TP 332

Saltzman B (1957) Equations governing the energetics of the larger scales of atmospheric turbulence in the domain of wave number. J Atmos Sci 14:513–523

Sud YC, Smith WE (1985) The influence of surface roughness of deserts on the July circulation (a numerical study). Boundary-Layer Meteorol 33:15–49

Trenberth KE (1985) Persistence of daily geopotential heights over the Southern Hemisphere. Mon Weather Rev 113:38–53

Trenberth KE, Olson JG (1988) ECMWF global analyses 1979–1986: Circulation statistics and data evaluation. NCAR Tech Note NCAR/TN-300+STR

Ulbrich U, Speth P (1991) The global energy cycle of stationary and transient atmospheric waves: results from ECMWF analyses. Meteorol Atmos Phys 45:125–138

von Storch H (1987) A statistical comparison with observations of control and El Niño simulations using the NCAR CCM. Beitr Phys Atmos 60:464–477

Weber S L, von Storch H, Viterbo P, Zambresky L (1993) Coupling an ocean wave model to an atmospheric general circulation model. Clim Dyn (in press)

Zwiers FW, von Storch H (1989) Multivariate recurrence analysis. Climate 2:1538–1553